Appearance of neutronization peak and decaying supernova neutrinos

Shin'ichiro Ando*
Department of Physics, School of Science, The University of Tokyo, 7-3-1 Hongo, Bunkyo-ku, Tokyo 113-0033, Japan
(Received 13 April 2004; published 17 August 2004)

Nonradiative neutrino decay, which is not satisfactorily constrained, possibly and significantly changes the detected neutrino signal from galactic supernova explosions. We focus on the appearance of a sharp peak due to a neutronization burst in the time profile; this phenomenon would occur if the original ν_e, produced at the neutrinosphere and becoming ν_2 or ν_3 at the stellar surface, decays into a lighter antineutrino state such as $\overline{\nu}_1$ or $\overline{\nu}_2$ coupled to $\overline{\nu}_e$. This is due to the fact that the signature of the neutronization burst is common to all numerical simulations, contrary to the spectral energy distribution of each flavor neutrino and antineutrino, which is still under intense debate. Therefore, the appearance of a neutronization peak in the $\overline{\nu}_e$ signal, if it were detected, would clearly indicate the nonstandard properties of neutrinos; the nonradiative neutrino decay would be one of the possible candidates. Using a newly developed formulation that includes flavor conversions inside the supernova envelope and neutrino decay during propagation in a vacuum, we calculate the expected neutrino signal at the detectors; the lifetimes of three modes τ_{12}, τ_{13}, and τ_{23} are taken to be free parameters. We further introduce simple quantities, which represent a peak sharpness of the time profile and spectral hardness, and investigate the parameter dependence of these quantities. As the result, it is found that they are quite dependent on the relevant parameters, but it would be quite difficult to distinguish models using the signal obtained by the Super-Kamiokande detector; the future megaton-class detectors would have sufficient sensitivity. We also compare the neutrino decay model with another mechanism—i.e., resonant spin-flavor conversion—which also may give the appearance of a neutronization peak, and conclude that these two independent mechanisms give a very different signal and one can be distinguished from the other.

DOI: 10.1103/PhysRevD.70.033004 PACS number(s): 95.85.Ry, 13.35.Hb, 14.60.Pq, 97.60.Bw

I. INTRODUCTION

In recent years, we have made great progress concerning our knowledge of neutrino properties; especially, many ground-based experiments, which observed atmospheric [1], solar [2], and reactor neutrinos [3], have revealed nonzero neutrino masses and mixing angles—i.e., properties beyond the standard model of particle physics. However, many other neutrino properties are left unknown, such as the nonzero magnetic moment and neutrino decay. Fortunately, our current knowledge of the mass differences as well as mixing angles enables us to consider these further exotic properties.

The most stringent and precise limits on both the neutrino magnetic moment and lifetime of nonradiative neutrino decay are obtained by solar neutrino observations. The basic technique for both cases is as follows. We already know that the famous solar neutrino problem is best explained by the large mixing angle (LMA) solution. If other mechanisms, such as the magnetic moment or nonradiative decay, work in nature, it should change the observed signal slightly; i.e., no positive claim can then be used to put a limit on the other exotic properties. For example, the neutrino magnetic moment, if ever, would produce $\overline{\nu}_e$ via spin-flavor precession inside the Sun [4,5]. However, the recent KamLAND experiment report that no $\overline{\nu}_e$ candidates were found from the Sun and this result is used to obtain the upper limit $\mu_\nu B_T(0.05R_\odot) \lesssim 10^{-5}\mu_B$ G, where μ_B is the Bohr magneton and B_T represents the transverse component of the solar magnetic field [6]. As for nonradiative neutrino decay, the lower limit to the lifetime is obtained to be $\tau_{12}/m \gtrsim 10^{-4}$ s/eV, owing to no positive signature of the decay in the flux and spectrum of the solar neutrinos [7] (see also Ref. [6] for a more recent and stringent limit using the KamLAND data). For other laboratory bounds, we refer the reader to Refs. [29,30].

These current limits are, however, still rather weak and such exotic mechanisms we consider potentially work in a more extreme environment as actually expected in the case of core collapse supernovas. Spin-flavor conversion of supernova neutrinos, induced by the interaction between the neutrino magnetic moment and the supernova magnetic fields, has been studied by many researchers [4,8–10] and found to give a leading effect on the neutrino spectrum and luminosity curve detected at the Earth. Also, in the case of neutrino decay, because galactic supernovas are expected to be located at a much more distant place compared with the Sun, a far more stringent lower limit to the lifetime is expected. In addition, it has recently been proposed that the diffuse background of neutrinos emitted by past supernova explosions may be used to probe the lifetime of neutrinos [11]. Thus, core-collapse supernovas are considered to be a wonderful astrophysical event, which can also be used as a laboratory for particle physics beyond the standard model. Other high-energy astrophysical objects are also expected to be available for this purpose [31].

However, the expected galactic supernova neutrino signal including nonradiative decay has not been discussed precisely; only very rough discussions have been done. Therefore, in the present paper, we give comprehensively the ex-

*Email address: ando@utap.phys.s.u-tokyo.ac.jp

pected supernova neutrino signal at the large volume water Cerenkov detectors on the Earth using realistic models of original neutrino spectrum and luminosity curve numerically calculated by Thompson *et al.* [12]. In particular, we focus on the case in which the sharp peak of a neutronization burst appears in the detected $\bar{\nu}_e$ signal at the water Čerenkov detectors. This is due to the original ν_e, produced by neutronization of the protoneutron star matter, possibly decays into $\bar{\nu}_e$ component during its propagation. In fact, in the previous paper we have pointed out that spin-flavor conversions in the supernova envelope can also cause the same phenomenon—i.e., the appearance of a neutronization peak in the $\bar{\nu}_e$ signal [9] (see also Ref. [10]). Hence, we compare the expected neutronization peak due to neutrino decay with that due to spin-flavor conversion and discuss their difference. Anyway, the appearance of such a signature clearly indicates a nonstandard neutrino property; in that case, neutrino decay would be one of the possible candidates. On the other hand, the obtained neutrino spectrum would be useful, but the shape of the original spectrum is still matter of debate. Although the difference among several groups is not very large, such a slight difference gives a large uncertainty when we discuss flavor conversion mechanisms or decay during propagation; i.e., whether the observed signature comes from the intrinsic or extrinsic effect (such as decay) would be quite unknown at present.

It should be noted that in this study we consider only vacuum neutrino decays. It is possible, however, to construct models where fast invisible decays can be triggered by matter effects [13–16] at the very high densities characterizing the supernova neutrinosphere, even in the absence of vacuum decays. In such scenarios, matter-induced decays (or interactions) might thus occur before flavor conversions in supernovas, leading to a phenomenology rather different from the one considered in this paper. We emphasize that the results discussed in the following sections are generally applicable to vacuum neutrino decay occurring after flavor transitions and our approach is not constrained from the supernova cooling discussion as detailed later. In addition, with the lifetime considered in this study, the flavor conversions occur well before the decay and mass eigenstates are expected to become incoherent. Thus, the interference effects between the two phenomena as discussed in Ref. [17] can be neglected in our treatment.

This paper is organized as follows. In Sec. II, we give several descriptions of models of decaying neutrinos and introduce a specific formulation of the decay rate from the Lagrangian. In Sec. III, an adopted model for the original (which means *before* occurring extrinsic processes such as flavor conversions or decays during propagation) spectrum and luminosity curve of supernova neutrinos are introduced; the effect of flavor conversions (without decay) is also described briefly. A newly developed formulation including both flavor conversions and decay is presented in Sec. IV, and we further give the calculated results obtained with the formulation in Sec. V. Finally, we discuss several other possibilities in Sec. VI and a brief summary is given in Sec. VII.

II. MODELS OF DECAYING NEUTRINOS

In this paper, we study nonradiative two-body decay of the "invisible mode"—i.e., decays into possibly detectable neutrinos plus truly invisible particles—e.g., light scalar or pseudoscalar bosons such as the Majoron [18]. On the other hand, radiative neutrino decay $\nu_j \to \nu_i \gamma$ has been considered in many papers (see Ref. [19] and references therein) and very stringent limits on the lifetime-to-mass ratio, $\tau/m \gtrsim 10^{20}$ s/eV, have already been set by several arguments [20]. The Majoron models that cause nonradiative neutrino decay typically have tree-level scalar or pseudoscalar couplings of the form

$$\mathcal{L} = g_{ij} \bar{\nu}_i \nu_j \chi + h_{ij} \bar{\nu}_j \gamma_5 \nu_j \chi + \text{H.c.}, \tag{1}$$

where χ represents a massless Majoron, which does not carry a definite lepton number. For the coupling specified by Eq. (1), the decay rates into neutrino and antineutrino daughters are given by [14,21]

$$\Gamma_{\nu_2 \to \nu_1} = \frac{m_1 m_2}{16\pi E_2} \left[g^2 \left(\frac{x}{2} + 2 + \frac{2}{x} \ln x - \frac{2}{x^2} - \frac{1}{2x^3} \right) + h^2 \left(\frac{x}{2} - 2 + \frac{2}{x} \ln x + \frac{2}{x^2} - \frac{1}{2x^3} \right) \right], \tag{2}$$

$$\Gamma_{\nu_2 \to \bar{\nu}_1} = \frac{m_1 m_2}{16\pi E_2} (g^2 + h^2) \left[\frac{x}{2} - \frac{2}{x} \ln x - \frac{1}{2x^3} \right], \tag{3}$$

where $x = m_2/m_1$, and we have dropped the subscripts on the coupling constants. Analogous expressions hold for $\bar{\nu}$ decay, with the replacements $\nu \leftrightarrow \bar{\nu}$. The decay widths in this paper are defined in the laboratory frame, and therefore the relation to the rest-frame lifetimes is $\Gamma(E) = m/(\tau E)$. From these two expressions (2) and (3) it is easily seen that the decay rate is dependent on whether the helicity flips or conserves as well as whether the neutrino masses are quasidegenerate ($x \approx 1$) or hierarchical ($x \gg 1$). In the case of strongly hierarchical masses, we obtain $\Gamma_{\nu_2 \to \nu_1} \approx \Gamma_{\nu_2 \to \bar{\nu}_1}$; on the other hand, in the case of quasidegenerate masses, Eqs. (2) and (3) lead to the relation $\Gamma_{\nu_2 \to \nu_1} \gg \Gamma_{\nu_2 \to \bar{\nu}_1}$, unless the coupling constant g is strongly suppressed compared with h. Therefore, if the neutrino masses are quasidegenerate, the produced neutrinos decay into neutrinos dominantly (helicity-conserved channel), while little into antineutrinos (helicity-flipped channel); hierarchical masses allow both decay channels by the same branching ratio.

The distribution of the energies of daughter (anti)neutrinos is very dependent on whether the masses are hierarchical or quasidegenerate. In the former case, the energy of daughter neutrinos is generally degraded, and its distribution is given by

$$\psi_c(E_p, E_d) = \frac{2E_d}{E_p^2}, \quad \psi_f(E_p, E_d) = \frac{2}{E_p} \left(1 - \frac{E_d}{E_p} \right), \tag{4}$$

where E_p and E_d represent the energy of parent and daughter neutrinos, respectively, and ψ_c and ψ_f are the distribution function of the helicity-conserved and helicity-flipped channels, respectively. In the latter case, on the other hand, the daughter neutrino energy is almost the same as that of parent neutrinos; the energy distribution becomes a delta function $\delta(E_p - E_d)$.

As already mentioned in Sec. I, we are mainly interested in the appearance of a neutronization peak at detectors, which dominantly catch $\bar{\nu}_e$; this is because the signature of the neutronization burst is very common to any supernova simulations, and its detection in the $\bar{\nu}_e$ channel would be a smoking gun to the nonstandard properties of neutrinos. Thus, the case of quasidegenerate masses, which prohibits the helicity-flipped channel—i.e., $\nu_e \to \bar{\nu}_e$, is not our prime interest. Although the obtained spectrum would also be helpful even in that case, we assume that the neutrino masses are strongly hierarchical ($m_1 \ll m_2 \ll m_3$) from this point on.

At the end of this section, we mention the constraints on the coupling constants g and h from the supernova cooling argument. In the dense core of supernovas, contrary to the decay in vacuum, the Majoron cooling proceeds mainly via $\nu_e \nu_e \to \chi$. A conservative upper limit on the coupling constant $|g_{ee}|$ is obtained by the fact that the luminosity of the Majoron, L_χ, should not exceed $3 \times 10^{53}\ \mathrm{erg\,s^{-1}}$ [16], because we already know that almost all the gravitational binding energy of new-born neutron stars is released as neutrinos by the actual detection of supernova neutrinos by Kamiokande [22] and IMB [23] detectors. This discussion translates into the bound $|g_{ee}| \lesssim 4 \times 10^{-7}$ and it is the strongest constraint on the parameter compared with other experimental ones such as of neutrinoless double-beta decay with Majoron emission [24]. Bounds on other parameters such as $|g_{e\mu}|$ and $|g_{\mu\mu}|$ are also obtained by similar arguments (for a detailed discussion, see, e.g., Ref. [16]). Our discussion in the present paper, however, is completely free of such stringent constraints. This is because the relevant parameters in our case are the coupling constants in the basis of mass eigenstates g_{ij}, while those in the cooling argument are in the basis of flavor eigenstates $g_{\alpha\beta}$. These two expressions in different bases are related to each other as

$$g_{ij} = \sum_{\alpha\beta} g_{\alpha\beta} U^*_{\alpha i} U_{\beta j}. \tag{5}$$

Since the mixing matrix $U_{\alpha i}$ contains several unknown parameters such as θ_{13} or the *CP*-violating phase δ, the limits from supernova cooling do not directly translate into g_{ij} relevant for our study.

III. ORIGINAL SUPERNOVA NEUTRINO SIGNAL AND FLAVOR CONVERSIONS

We adopt as the original neutrino spectrum as well as the luminosity curve, the results of the numerical simulation by Thompson *et al.* [12]; we use the model calculated for the $15M_\odot$ progenitor star. Their calculation has particularly focused on shock breakout and followed the dynamical evolution of the cores through collapse until the first 250 ms after core bounce. They have incorporated all the relevant neutrino processes such as neutrino-nucleon scatterings with nucleon recoil as well as nucleon bremsstrahlung; these reactions have recently been recognized to give a nonnegligible contribution to the spectral formation. In Figs. 1 and 2, we show the original luminosity curve and number spectrum of neutrinos, respectively. In these figures, ν_x represents nonelectron neutrinos and antineutrinos.

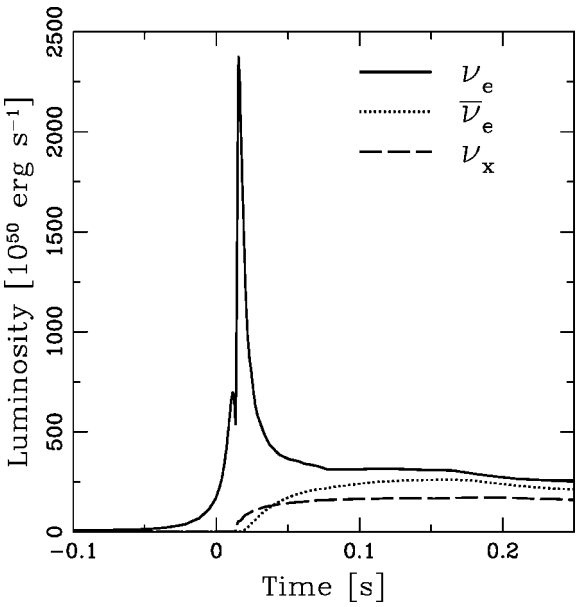

FIG. 1. Original luminosity of the emitted neutrinos as a function of time, calculated by Thompson *et al.* [12]. The progenitor mass is $15M_\odot$.

The neutrino luminosity curve is quite characteristic

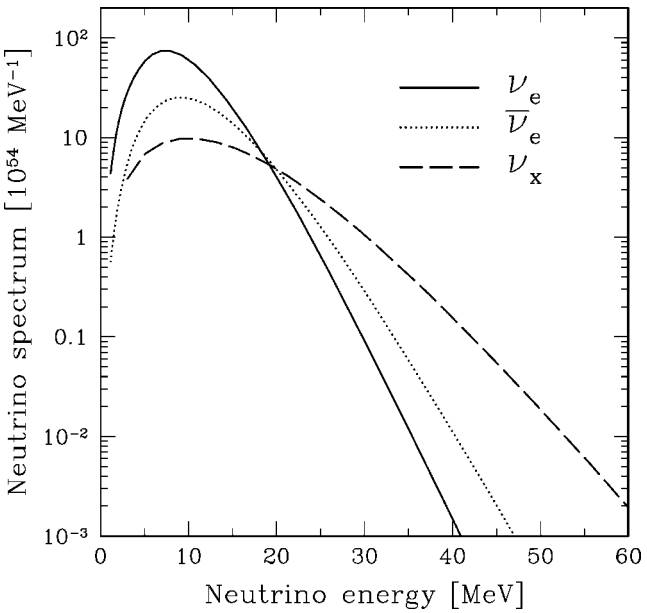

FIG. 2. Original neutrino spectrum integrated to 0.25 s after core bounce, calculated by Thompson *et al.* [12]. The progenitor mass is $15M_\odot$.

among the different flavors. In particular, there is a very sharp peak of ν_e called the neutronization burst, whose duration is typically ~ 10 ms and peak luminosity is $\sim 10^{53}$ erg s^{-1}. This strong peak is illustrated as follows. As a supernova shock moves outward, it dissociates nuclei into free nucleons, which triggers the deleptonization process $e^- p \to \nu_e n$; these ν_e build up a sea because they are trapped and advected with matter. When the shock crosses the ν_e neutrinosphere, within which the created ν_e are trapped, they are abruptly emitted. For the other flavors $\bar{\nu}_e$ and ν_x, there is no such sudden burst; both luminosities glow rather gradually and they are similar to each other.

The other characteristic that provides information on the flavor conversion mechanism as well as neutrino decay is the hierarchy of the average energy $\langle E_{\nu_e}\rangle < \langle E_{\bar{\nu}_e}\rangle < \langle E_{\nu_x}\rangle$ as clearly seen from Fig. 2; neutrino flavor conversion and decay also change the spectral shape. This energy hierarchy is explained as follows. Since ν_x interacts with matter only through neutral-current interactions in supernovas, they are weakly coupled with matter compared to ν_e and $\bar{\nu}_e$. Thus the neutrinosphere of ν_x is located deeper in the core than that of ν_e and $\bar{\nu}_e$, which leads to higher temperatures for ν_x. The difference between ν_e and $\bar{\nu}_e$ comes from the fact that the core is neutron rich and the ν_e couples with matter more strongly, through the $\nu_e n \to e^- p$ reaction.

Although we only use one specific model [12], the signature of the neutronization burst appears in all reliable numerical simulations. It is quite natural that the height and width of such a peak are dependent on supernova parameters as well as numerical approaches. However, we are not interested in such a slight difference but focus only on the rough signature—i.e., the *appearance or absence* of a neutronization peak in the $\bar{\nu}_e$ channel. We cannot discuss in any details without a concrete and reliable original model, but even such rough information, if ever detected, would bring a very fruitful and novel perspective to particle physics. As for the neutrino spectrum, there is a general tendency of the hierarchy of the average energies—i.e., $\langle E_{\nu_e}\rangle < \langle E_{\bar{\nu}_e}\rangle < \langle E_{\nu_x}\rangle$ as already noted—and this tendency seems to be common to almost all numerical calculations. However, the spectral shape and especially the average energy ratio between $\bar{\nu}_e$ and ν_x are still matter of controversy, and we cannot conclude that the spectral information at the detectors would be very useful at present (see, for a comparison among several calculations, Ref. [25]). Contrary to the luminosity curve, the neutrino spectrum does not indicate such a prominent signature as a neutronization burst, and therefore, the obtained spectrum would be of secondary importance for the purpose of this study. In the near future, however, the situation may become significantly better, especially if some process relevant for successful supernova explosions were discovered in computers; in that case, the spectrum as well as luminosity curve would be very useful to precisely obtain the unknown property of neutrinos.

Before moving on to a discussion including neutrino decay, here we shortly describe the flavor conversions inside the supernova envelope *without* any other processes such as decay. Neutrinos of different mass eigenstates are expected to be incoherent with each other when they reach the detector, and then the number intensity (i.e., number per area, time, energy, and solid angle) of $\bar{\nu}_e$ can be simply represented by

$$I^-_{\nu_e}(L) = |U_{e1}|^2 I^-_{\nu_1}(R_{\rm SN}) + |U_{e2}|^2 I^-_{\nu_2}(R_{\rm SN}) + |U_{e3}|^2 I^-_{\nu_3}(R_{\rm SN})$$

$$\simeq \cos^2\theta_{12} I^-_{\nu_1}(R_{\rm SN}) + \sin^2\theta_{12} I^-_{\nu_2}(R_{\rm SN}), \qquad (6)$$

where L and $R_{\rm SN}$ represent the distance to and radius of the supernova, respectively. The second equality comes from the fact that the value of θ_{13} is constrained to be negligibly small from reactor neutrino experiments [26] and $\theta_{23} \simeq \pi/4$; from the solar and reactor neutrino observation the obtained value for θ_{12} is $\cos^2\theta_{12} \simeq 0.7$ (LMA solution) [2,3]. The intensity at the supernova surface $I_\nu(R_{\rm SN})$ reflects the flavor conversions during propagation inside the supernova envelope. Flavor conversions during neutrino propagation have been extensively studied by many researchers (see, e.g., Ref. [27]), but we briefly summarize them here. In the case of a normal mass hierarchy ($m_1 \ll m_3$), on which we focus in this study, the intensity of each mass eigenstate at the surface is fairly well known to be

$$I^-_{\nu_1}(R_{\rm SN}) = I^-_{\bar{\nu}_e}(0),$$

$$I^-_{\nu_2}(R_{\rm SN}) = I^-_{\nu_3}(R_{\rm SN}) = I_{\nu_x}(0), \qquad (7)$$

where $I_\nu(0)$ represents the neutrino intensity of each flavor eigenstate at the neutrinosphere, for which we use the results of numerical simulation shown in Figs. 1 and 2. By a combination of Eqs. (6) and (7), we can see that owing to flavor conversion inside the supernova, about 30% of the detected $\bar{\nu}_e$ would originate from ν_x at production; this would harden the obtained spectrum at the detectors. On the other hand, for the neutrino sector, the final expression for the intensity of ν_e is given by the same expression as Eq. (6) but with replacing $\bar{\nu}$ by ν. Flavor conversions inside the supernova envelope are, this time, a little bit complicated; the unknown parameter θ_{13} strongly affects the results. Instead of θ_{13}, we rather use so-called ''flip probability'' at the higher resonance point P_H [27], which equals 0 (1) when $\sin^2 2\theta_{13} \gtrsim 10^{-3}$ ($\sin^2 2\theta_{13} \lesssim 10^{-5}$). The expressions corresponding to Eq. (7) for the neutrino sector are then given by

$$I_{\nu_1}(R_{\rm SN}) = I_{\nu_x}(0),$$

$$I_{\nu_2}(R_{\rm SN}) = P_H I_{\nu_e}(0) + (1-P_H) I_{\nu_x}(0),$$

$$I_{\nu_3}(R_{\rm SN}) = (1-P_H) I_{\nu_e}(0) + P_H I_{\nu_x}(0). \qquad (8)$$

These expressions are necessary for estimating the neutrino flux in the case of possible decay, since $\nu_i \to \bar{\nu}_j$ might occur.

IV. FORMULATION

In this section, we derive new formulation for the detected $\bar{\nu}_e$ flux, which includes both flavor conversion and decay during propagation. The $\bar{\nu}_e$ intensity at the detectors is represented by

$$I^-_{\nu_e}(L,E)=|U_{e1}|^2 I^-_{\nu_1}(L,E)+|U_{e2}|^2 I^-_{\nu_2}(L,E) +|U_{e3}|^2 I^-_{\nu_3}(L,E), \tag{9}$$

which is similar to Eq. (6), but the intensity of the specific mass eigenstate is no longer conserved during its propagation owing to decay, $I^-_{\nu_i}(L)\neq I^-_{\nu_i}(R_{\rm SN})$. Here and from this point on, we explicitly show the neutrino energy E. The effect of neutrino decay on the intensity of each mass eigenstate $\bar{\nu}_i$ is included by adding the appearance and disappearance terms to the transfer equation—i.e.,

$$\frac{dI^-_{\nu_i}}{dr}=-\sum_{j<i}\Gamma_{ji}(E)I^-_{\nu_i}(r,E) +\sum_{j>i}\int_E^\infty dE'[\psi_c(E',E)\Gamma^-_{\nu_j\to\nu_i}(E')I^-_{\nu_j}(r,E') +\psi_f(E',E)\Gamma_{\nu_j\to\bar{\nu}_i}(E')I_{\nu_j}(r,E')], \tag{10}$$

where we define $\Gamma_{ji}=\Gamma^-_{\nu_i\to\nu_j}+\Gamma^-_{\bar{\nu}_i\to\bar{\nu}_j}$, etc. A similar formulation holds for the neutrino sector, although we do not show it explicitly. The first and second sums of Eq. (10) reflect the disappearance and appearance of $\bar{\nu}_i$, respectively. Fortunately, this set of formulations can be analytically integrated from $R_{\rm SN}$ to L. In the case of three-flavor context and normal mass hierarchy, the solution to Eq. (10) is given by

$$I^-_{\nu_1}(L,E)=I^-_{\nu_1}(R_{\rm SN},E) +\int_E^\infty dE'\left[\frac{1-e^{-[\Gamma_{13}(E')+\Gamma_{23}(E')]L}}{\Gamma_{13}(E')+\Gamma_{23}(E')}J_{3\to1}(E',E) +\frac{1-e^{-\Gamma_{12}(E')L}}{\Gamma_{12}(E')}J_{2\to1}(E',E) +\int_{E'}^\infty dE''\left(\frac{1-e^{-\Gamma_{12}(E')L}}{\Gamma_{12}(E')} -\frac{1-e^{-[\Gamma_{13}(E'')+\Gamma_{23}(E'')]L}}{\Gamma_{13}(E'')+\Gamma_{23}(E'')}\right)J_{3\to2\to1}(E'',E',E)\right], \tag{11}$$

$$I^-_{\nu_2}(L,E)=e^{-\Gamma_{12}(E)L}I^-_{\nu_2}(R_{\rm SN},E) +\int_E^\infty dE'\frac{e^{-\Gamma_{12}(E)L}-e^{-[\Gamma_{13}(E')+\Gamma_{23}(E')]L}}{\Gamma_{13}(E')+\Gamma_{23}(E')-\Gamma_{12}(E)} \times J_{3\to2}(E',E), \tag{12}$$

$$I^-_{\nu_3}(L,E)=e^{-[\Gamma_{13}(E)+\Gamma_{23}(E)]L}I^-_{\nu_3}(R_{\rm SN},E), \tag{13}$$

where

$$J_{3\to2\to1}(E'',E',E)=\frac{1}{\Gamma_{13}(E'')+\Gamma_{23}(E'')-\Gamma_{12}(E')} \times[\psi_c(E',E)\Gamma^-_{\nu_2\to\nu_1}(E')J_{3\to2}(E'',E') +\psi_f(E',E)\Gamma_{\nu_2\to\bar{\nu}_1}(E')\tilde{J}_{3\to2}(E'',E')], \tag{14}$$

$$J_{i\to j}(E',E)=\psi_c(E',E)\Gamma^-_{\nu_i\to\nu_j}(E')I^-_{\nu_i}(R_{\rm SN},E') +\psi_f(E',E)\Gamma_{\nu_i\to\bar{\nu}_j}(E')I_{\nu_i}(R_{\rm SN},E'), \tag{15}$$

$$\tilde{J}_{i\to j}(E',E)=\psi_c(E',E)\Gamma_{\nu_i\to\nu_j}(E')I_{\nu_i}(R_{\rm SN},E') +\psi_f(E',E)\Gamma^-_{\bar{\nu}_i\to\nu_j}(E')I^-_{\nu_i}(R_{\rm SN},E'). \tag{16}$$

In these expressions, we have used the assumption that $\Gamma_{ij}R_{\rm SN}\ll1$; i.e., neutrinos never decay during their propagation inside the supernova envelope. With this assumption, the intensity at the stellar surface $I_\nu(R_{\rm SN},E)$ is, also in this case, represented by Eqs. (7) and (8). Thus we obtain the intensity of $\bar{\nu}_e$ at the detector using Eqs. (9), (11)–(16), (7), and (8).

Although we have given a quite general expression, we are rather interested in the more specific case, in which the neutronization peak appears in the $\bar{\nu}_e$ channel; this is realized when the neutrino masses are strongly hierarchical as already discussed in Secs. II and III. In this case, we obtain $\Gamma^-_{\nu_i\to\nu_j}=\Gamma^-_{\bar{\nu}_i\to\bar{\nu}_j}=\Gamma_{ji}/2$, etc., and the energy distribution factions are given by Eq. (4). From this point on, we use τ_{12}/m, τ_{13}/m, and τ_{23}/m as free parameters, which are related to Γ_{ij} by $\Gamma_{ij}(E)=m/(\tau_{ij}E)$.

V. RESULTS

The obtained number flux and fluence (time-integrated flux) of $\bar{\nu}_e$, using Eqs. (9), (11)–(16), (7), and (8) are shown in Figs. 3–6. In the inset of each figure, we show the expected number of detection at the water Cerenkov detectors with a fiducial volume of 640 kton [20 times larger than that of the Super-Kamiokande (SK) detector], by assuming that the supernova occurred at 10 kpc. The values labeled in the vertical axis could be rescaled by using a factor of $(10\ {\rm kpc}/D)^2(V_{\rm fid}/640\ {\rm kton})$ in other cases, where D represents the distance and $V_{\rm fid}$ the fiducial volume. The cross section for the dominant catching process $\bar{\nu}_e p\to e^+ n$ is fairly well understood and we used that given in Ref. [28]. In addition we have used the trigger threshold expected to be installed to SK-III (after full repair); with this threshold the electrons and positrons of the energy of 3 MeV can be detected at 100% efficiency. We neglect all other processes

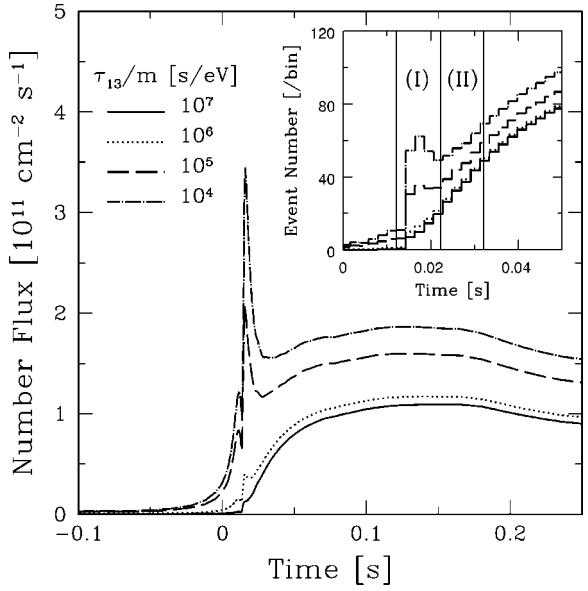

FIG. 3. Energy-integrated flux at the Earth in the case of adiabatic conversion ($P_H=0$), for various values of τ_{13}/m. The other parameters (τ_{12}/m and τ_{23}/m) are set to infinity. The expected number of events at the detector of 640 kton is shown in the inset.

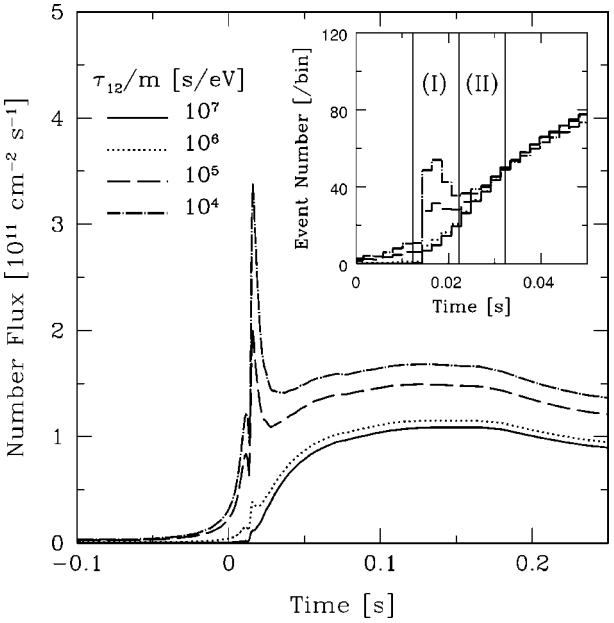

FIG. 5. The same as Fig. 3 but for the case of nonadiabatic conversion ($P_H=1$), for various values of τ_{12}/m with fixed τ_{13}/m and τ_{23}/m to infinity.

such as electron scattering because of their subdominance.

Figures 3 and 4 indicate the energy- and time-integrated flux, respectively, in the case of the adiabatic conversion—i.e., $P_H=0$. The fluxes are evaluated for various values of τ_{13}/m with τ_{12}/m and τ_{23}/m fixed to infinity. The shape of the luminosity curve is found to strongly depend on the lifetime of the $\nu_3(\overline{\nu}_3)\to\overline{\nu}_1$ mode. This is because in the case of adiabatic conversion, the original ν_e becomes ν_3 at the stellar surface [Eq. (8)] and they decay into $\overline{\nu}_1$, which dominantly couple to $\overline{\nu}_e$. Thus, the peak of the neutronization burst clearly appears at the detectors for $\tau_{13}/m<10^5$ s/eV. As for the spectrum, the energies of daughter neutrinos are significantly degraded as shown in Fig. 4 and give a very characteristic signature. However, since the cross section is roughly proportional to E^2 and highly insensitive to low-energy neutrinos, the expected event number is almost the

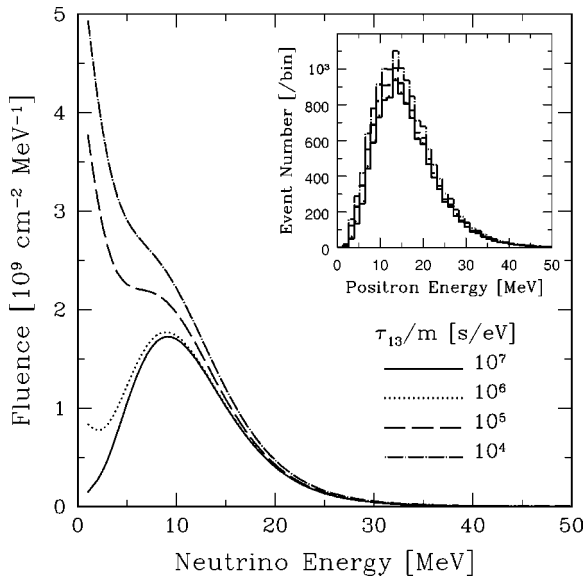

FIG. 4. Fluence (time-integrated flux) at the Earth in the case of adiabatic conversion ($P_H=0$), for various values of τ_{13}/m. The other parameters (τ_{12}/m and τ_{23}/m) are set to infinity. The expected number of events at the detector of 640 kton is shown in the inset.

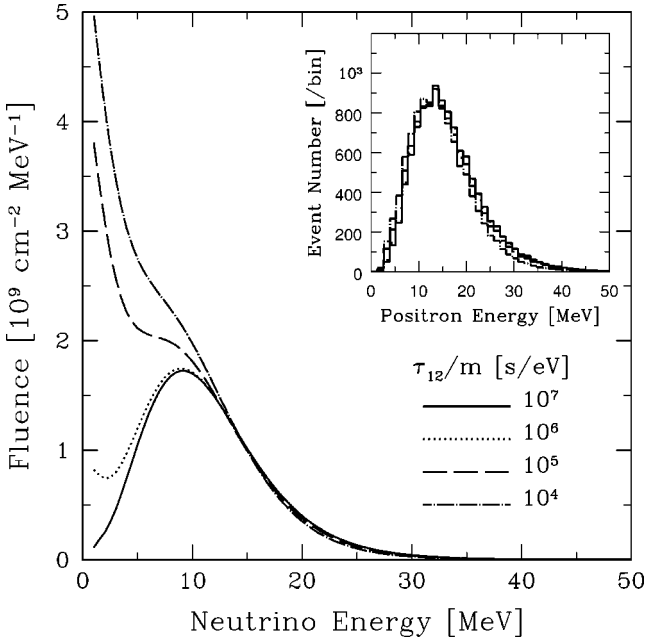

FIG. 6. The same as Fig. 4 but for the case of nonadiabatic conversion ($P_H=1$), for various values of τ_{12}/m with fixed τ_{13}/m and τ_{23}/m to infinity.

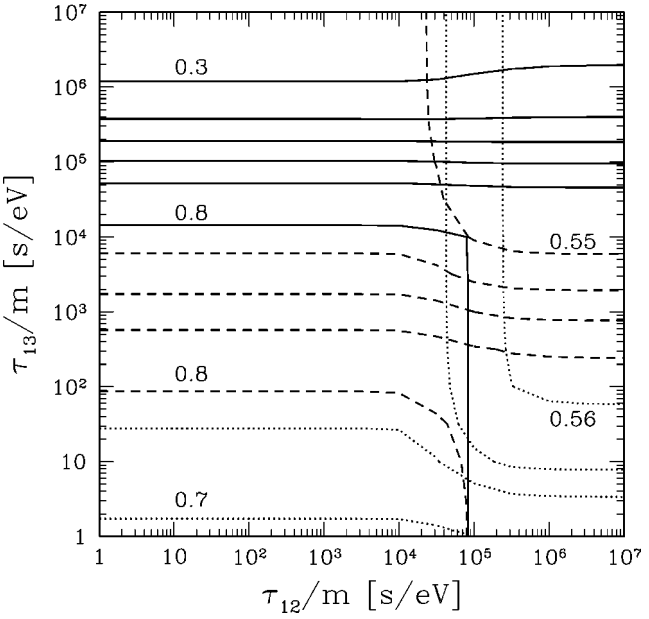

FIG. 7. Contour plot of R_T against the $(\tau_{12}/m, \tau_{13}/m)$ plane, in the case of the adiabatic conversion $(P_H=0)$. The values of τ_{23}/m are taken to be 10^7 (solid curves), 10^3 (dashed curves), and 1 (dotted curves) s/eV. Each curve of the same type is equally spaced by the value of R_T with the indicated largest and smallest values.

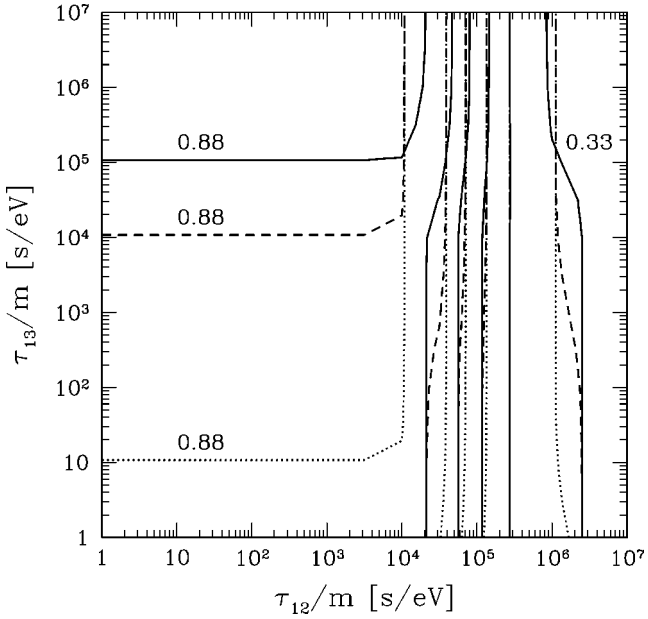

FIG. 8. The same as Fig. 7 but for the case of the nonadiabatic conversion $(P_H=1)$.

same at such a low-energy region as shown in the inset of Fig. 4. This degradation of the neutrino energy due to its decay also causes the actually detected neutronization peak to be less prominent compared to that seen in the flux.

The case of nonadiabatic conversion $(P_H=1)$ is shown correspondingly in Figs. 5 and 6. This time, the relevant parameter is changed to τ_{12}/m because ν_e created by the neutronization is converted into ν_2 at the stellar surface. The characteristics appearing in both the luminosity curve and spectrum are similar to those in the case of adiabatic conversion, but the total event number is slightly smaller. This difference comes from the fact that the detected $\overline{\nu}_e$ is coupled to $\overline{\nu}_2$ by $\sim 30\%$ [Eq. (9)] and the $\overline{\nu}_2$ disappears owing to its decay. On the other hand, the disappearance of $\overline{\nu}_3$ does not directly affect the expected event number since they hardly couple to $\overline{\nu}_e$.

In order to discuss the parameter dependence of this mechanism, we simply define the following quantity, which represents the peak sharpness of the time profile. Namely, it is defined as

$$R_T = \frac{\text{event number in region (I)}}{\text{event number in region (II)}}, \tag{17}$$

where regions (I) and (II) are defined in the insets of Figs. 3 and 5. A larger value for R_T means that the peak of neutronization burst is more prominent. We plot the contour map of R_T against the values of τ_{12}/m and τ_{13}/m assuming several values for τ_{23}/m; the result in the case of adiabatic (nonadiabatic) conversion is shown in Fig. 7 (Fig. 8). In both figures, the solid, dashed, and dotted curves represent the case that the values of τ_{23}/m are 10^7 (essentially no decay due to the $3\rightarrow 2$ mode), 10^3, and 1 s/eV, respectively. Each curve of the same type is plotted at an equally spaced level, while the largest and smallest values are indicated. It can be clearly seen that in the case of $P_H=0$, the R_T is strongly dependent on the parameter τ_{13}/m but highly insensitive to τ_{12}/m. This point also holds for the nonadiabatic case with the corresponding replacement, $\tau_{13}\leftrightarrow\tau_{12}$.

VI. DISCUSSION

In order to discuss how to discriminate one from the other decaying models, in addition to R_T, we use another quantity that represents the spectral hardness:

$$R_E = \frac{\text{event number for } E_e > 25 \text{ MeV}}{\text{event number for } E_e < 15 \text{ MeV}}. \tag{18}$$

The values for R_E are obtained from the detected spectrum—i.e., from the insets of Figs. 4 and 6. As already discussed in Sec. III, because the average energy difference between each flavor neutrino is still a matter of controversy, the obtained spectrum would be also affected by such uncertainties. We believe, however, that our treatment is quite reasonable, since using the simple quantity R_E would make the discussion rather insensitive to such unsettled details.

Figure 9 shows the location of each model on the (R_E, R_T) plane for the adiabatic case. We also show the 1σ statistical error bars of R_E and R_T; the size of these errors changes as $(D/10 \text{ kpc})(V_{\text{fid}}/640 \text{ kton})^{-1/2}$ in other cases. Labels such as "$2\rightarrow 1$" represent the relevant decaying mode, while the other modes are assumed to be stable; the label "All" represents the case that $\tau_{12}/m=\tau_{13}/m=\tau_{23}/m$. Points of the same symbol show how their location changes with lifetime; each point of one symbol represents a model with a specific value of lifetime-to-mass ratio τ/m, which is

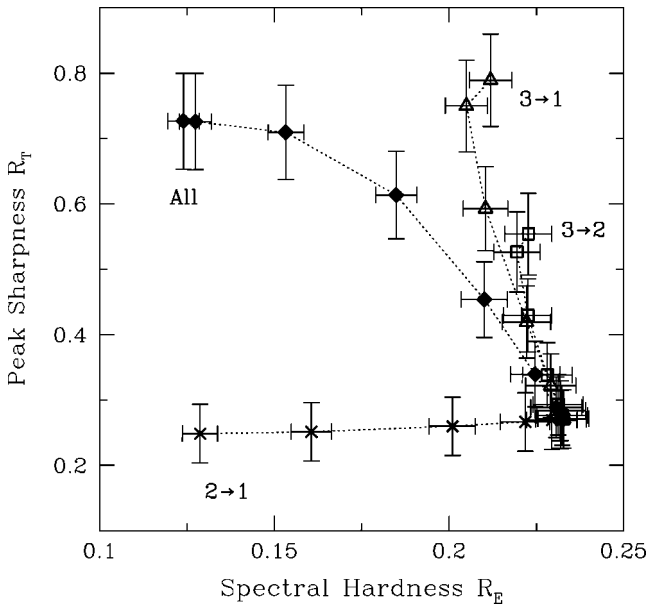

FIG. 9. Neutrino decay model plotted on the (R_E, R_T) plane in the case of adiabatic conversion. The error bars include only statistical errors, and are at the 1σ level, but their size should be accordingly rescaled as $(D/10\ \mathrm{kpc})(V_{\mathrm{fid}}/640\ \mathrm{kton})^{-1/2}$. The labels represent the relevant mode (see text) and points of the same symbol indicate the model with a specific value of τ/m, which is equally spaced from 10^4 to 10^7 s/eV, logarithmically.

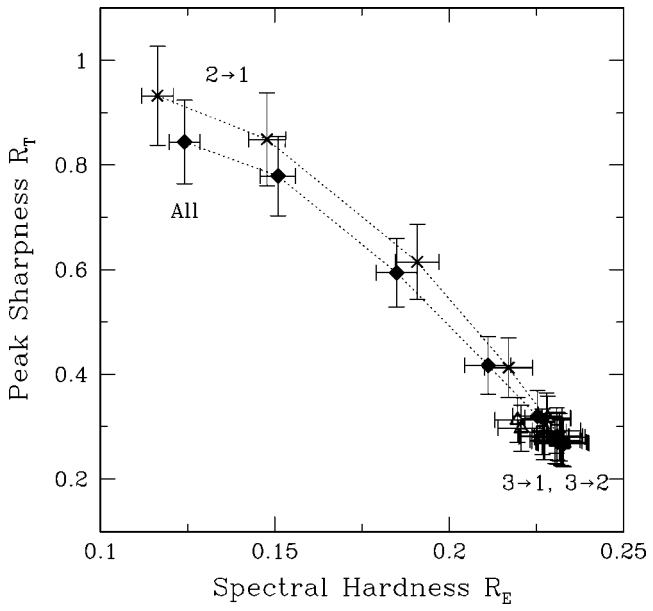

FIG. 10. The same as Fig. 9, but in the case of nonadiabatic conversion.

equally spaced (logarithmically) from 10^4 to 10^7 s/eV. The dotted lines connect these points just to guide our eyes. All the modes are degenerate when $\tau/m = 10^7$ s/eV at $R_E = 0.23$ and $R_T = 0.27$, which means that there occurs essentially no decay. From this figure, models with extreme parameter values can be distinguished from one another, if the currently planned megaton-class detectors, such as Hyper-Kamiokande and UNO, detected the galactic supernova neutrino burst. On the other hand, in the case of currently working detectors such as SK, the errors become very large by a factor of $\geqslant \sqrt{20}$, and even using these very simple quantities R_E and R_T, it would be quite difficult to derive some information.

We here briefly illustrate the behavior of each model, shown in Fig. 9. As already discussed in the previous section, the decaying mode from $\nu_3(\bar{\nu}_3)$ to $\bar{\nu}_1$ makes the value of R_T larger owing to the appearance of a neutronization peak. A similar explanation applies to the $3 \to 2$ mode but its prominence is reduced because the $\bar{\nu}_2$ state included in the $\bar{\nu}_e$ is smaller compared to $\bar{\nu}_1$ state. The $2 \to 1$ mode does not change the peak sharpness R_T, since in the case of adiabatic conversion, the $\nu_2(\bar{\nu}_2)$ at the stellar surface does not contain any component from the original ν_e. Instead of an almost constant R_T, the spectral hardness R_E significantly changes with the value of τ_{12}/m. This is also easily illustrated as follows. At the supernova surface, the ν_2 and $\bar{\nu}_2$ both originate from ν_x, which shows the hardest spectral shape. Without any decay, the obtained $\bar{\nu}_e$ signal then contains an $\sim 30\%$ amount of the original ν_x. On the contrary, if the decaying mode $2 \to 1$ were relevant, the original ν_x component, which otherwise should contribute to the $\bar{\nu}_e$ spectrum, would disappear and instead it would appear as $\bar{\nu}_1$ but with a significantly reduced energy; this makes the spectral hardness R_E considerably small. The "All" model, in which we assumed $\tau_{12}/m = \tau_{13}/m = \tau_{23}/m$, includes both effects given above; i.e., the peak sharpness R_T increases owing to the $3 \to 1$ and $3 \to 2$ modes, while the spectral hardness R_E decreases owing to the $2 \to 1$ mode.

Figure 10 is the same as Fig. 9, but for the case of nonadiabatic conversion $P_H = 1$. In this case, the decaying mode from ν_3 and $\bar{\nu}_3$ does not essentially change the expected signal, because they are not coincident with the original ν_e at the stellar surface as well as having essentially no coupling to $\bar{\nu}_e$. The original ν_e, instead, in this case, appears as ν_2; thus the decaying mode $2 \to 1$ considerably changes the detected signals.

There also exists another mechanism that possibly changes the original ν_e into a detected $\bar{\nu}_e$, resulting in the appearance of a sharp peak due to a neutronization burst at the detectors—i.e., resonant spin-flavor (RSF) conversion [9,10]. This mechanism is induced by the interaction between a supernova magnetic field and the Majorana magnetic moment of neutrinos. According to Ref. [9], the very sharp peak of a neutronization burst could appear owing to the combination effect of the RSF and ordinary matter-induced conversion, if the following conditions are all satisfied: (i) the mass hierarchy is inverted, (ii) the value of θ_{13} is sufficiently large, and (iii) the neutrino magnetic moment as well as supernova magnetic field is large enough to induce the adiabatic RSF conversion (but see also Ref. [10]). In order to compare the RSF mechanism with the decaying models, we plot the model groups given in Ref. [9] in Fig. 11. For comparison we also plot the decaying models with $\tau/m = 10^4$ s/eV and $P_H = 0$. The models with $\tau/m = 10^7$ s/eV

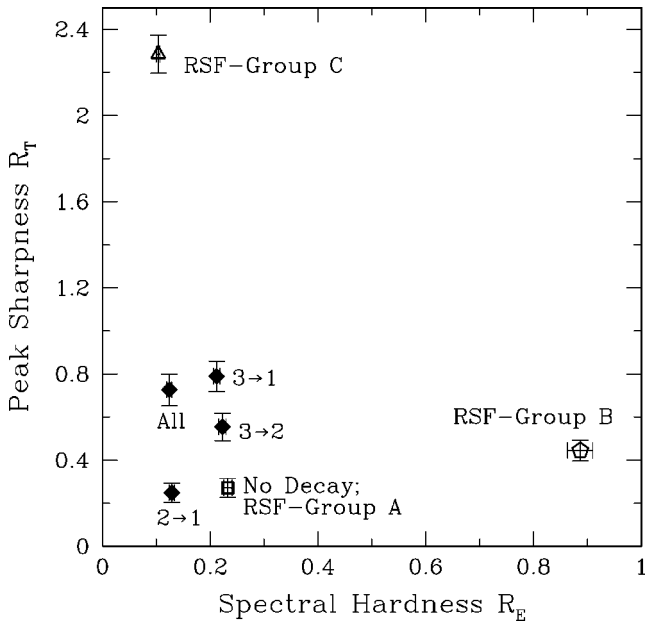

FIG. 11. Model groups A, B, and C due to the RSF mechanism given in Ref. [9], plotted on the (R_E, R_T) plane. The decaying models for the adiabatic conversion with $\tau/m = 10^4$ s/eV are also plotted for comparison.

(no-decay model) are degenerate with group A due to the RSF conversion. This figure clearly indicates that the RSF mechanism potentially gives a far more characteristic $\bar{\nu}_e$ signal at the detectors; both the peak sharpness of time profile R_T (group C) and spectral hardness R_E (group B) are very prominent, and even the SK detector enables us to discriminate these model groups.

VII. CONCLUSIONS

Nonradiative decay of neutrinos is not constrained sufficiently; the most stringent lower limit to the lifetime τ_{12} is obtained from the solar neutrino observation but it is very weak [7]. Thus, neutrino decay possibly affects the neutrino signal from other astrophysical objects such as supernovas.

Using newly derived formulation, which includes both flavor conversions inside the supernova envelope and neutrino decays during propagation in vacuum, we calculated the expected neutrino luminosity curve as well as the spectrum at future large volume water Čerenkov detectors. In these calculations, we particularly focused on the decaying model such that the original ν_e appears in the $\bar{\nu}_e$ signal as the result of flavor conversion and decay. This is because such a situation can give the appearance of a sharp peak in the time profile due to the neutronization burst, and it could be easily recognized. We discuss that this actually may be realized if the neutrino masses are strongly hierarchical, and we have assumed it in actual calculations. The lifetimes of three decaying modes, τ_{12}, τ_{13}, and τ_{23}, are taken to be free parameters, and the cases of adiabatic and nonadiabatic conversions are treated independently. The results of the calculations are shown in Figs. 3–6 and the neutronization peak can be significantly prominent in future megaton-class water Čerenkov detectors.

In order to discuss the parameter dependence of the neutrino signal, we introduce the rather simple quantities R_T and R_E, which represent the peak sharpness and spectral hardness, respectively. As shown in Figs. 7 and 8, the value of R_T is strongly dependent on the value of P_H as well as the relevant lifetime. From Figs. 9 and 10, we see that the behaviors of each model on the (R_E, R_T) plane are considerably different from one another. But we also show that the location of these decay models on this plane does not give prominent properties enough for us to distinguish using current detectors such as SK, on the contrary to a very significant dispersion due to the RSF conversion (Fig. 11). Finally, we again stress that the appearance of the neutronization peak clearly indicates nonstandard properties of neutrinos; neutrino decay would then be one of the possible candidates.

ACKNOWLEDGMENT

This work was supported by a Grant-in-Aid from the JSPS.

[1] The Super-Kamiokande Collaboration, Y. Fukuda *et al.*, Phys. Rev. Lett. **82**, 2644 (1999).

[2] The Super-Kamiokande Collaboration, S. Fukuda *et al.*, Phys. Lett. B **539**, 179 (2002); SNO Collaboration, S.N. Ahmed *et al.*, Phys. Rev. Lett. **92**, 181301 (2004).

[3] KamLAND Collaboration, K. Eguchi *et al.*, Phys. Rev. Lett. **90**, 021802 (2003).

[4] C.S. Lim and W.J. Marciano, Phys. Rev. D **37**, 1368 (1988); E.Kh. Akhmedov, Sov. J. Nucl. Phys. **48**, 382 (1988); Phys. Lett. B **213**, 64 (1988).

[5] C.S. Lim, M. Mori, Y. Oyama, and A. Suzuki, Phys. Lett. B **243**, 389 (1990); R.S. Raghavan, A.B. Balantekin, F. Loreti, A.J. Baltz, S. Pakvasa, and J. Pantaleone, Phys. Rev. D **44**, 3786 (1991); E.Kh. Akhmedov, Phys. Lett. B **255**, 84 (1991); R. Barbieri, G. Fiorentini, G. Mezzorani, and M. Moretti, *ibid.* **259**, 119 (1991); E.Kh. Akhmedov, A. Lanza, and S.T. Petcov, *ibid.* **348**, 124 (1995); S. Pastor, V.B. Semikoz, and J.W.F. Valle, *ibid.* **423**, 118 (1998); E.Kh. Akhmedov and J. Pulido, *ibid.* **553**, 7 (2003).

[6] KamLAND Collaboration, K. Eguchi *et al.*, Phys. Rev. Lett. **92**, 071301 (2003).

[7] J.F. Beacom and N.F. Bell, Phys. Rev. D **65**, 113009 (2002); A. Bandyopadhyay, S. Choubey, and S. Goswami, Phys. Lett. B **555**, 33 (2003).

[8] M.B. Voloshin, Phys. Lett. B **209**, 360 (1988); E.Kh. Akhmedov and Z.G. Berezhiani, Nucl. Phys. **B373**, 479 (1992); E.Kh. Akhmedov, S.T. Petcov, and A.Yu. Smirnov, Phys. Rev. D **48**, 2167 (1993); J.T. Peltoniemi, Astron. Astrophys. **254**, 121 (1992); H. Athar, J.T. Peltoniemi, and A.Yu. Smirnov, Phys. Rev. D **51**, 6647 (1995); T. Totani and K. Sato, *ibid.* **54**, 5975

(1996); H. Nunokawa, Y.Z. Qian, and G.M. Fuller, *ibid.* **55**, 3265 (1997); H. Nunokawa, R. Tomàs, and J.W.F. Valle, Astropart. Phys. **11**, 317 (1999); S. Ando and K. Sato, Phys. Rev. D **67**, 023004 (2003); **68**, 023003 (2003).

[9] S. Ando and K. Sato, J. Cosmol. Astropart. Phys. **10**, 001 (2003).

[10] E.Kh. Akhmedov and T. Fukuyama, J. Cosmol. Astropart. Phys. **12**, 007 (2003).

[11] S. Ando, Phys. Lett. B **570**, 11 (2003); G.L. Fogli, E. Lisi, A. Mirizzi, and D. Montanino, Phys. Rev. D **70**, 013001 (2004).

[12] T.A. Thompson, A. Burrows, and P. Pinto, Astrophys. J. **592**, 434 (2003).

[13] Z.G. Berezhiani and M.I. Vysotsky, Phys. Lett. B **199**, 281 (1987).

[14] Z.G. Berezhiani, G. Fiorentini, M. Moretti, and A. Rossi, Z. Phys. C **54**, 581 (1992); C. Giunti, C.W. Kim, U.W. Lee, and W.P. Lam, Phys. Rev. D **45**, 1557 (1992).

[15] M. Kachelriess, R. Tomàs, and J.W.F. Valle, Phys. Rev. D **62**, 023004 (2000); Z.G. Berezhiani and A.Yu. Smirnov, Phys. Lett. B **220**, 279 (1989); K. Choi and A. Santamaria, Phys. Rev. D **42**, 293 (1990); R. Tomàs, H. Päs, and J.W.F. Valle, *ibid.* **64**, 095005 (2001); R.S. Raghavan, X.-G. He, and S. Pakvasa, *ibid.* **38**, 1317 (1988).

[16] Y. Farzan, Phys. Rev. D **67**, 073015 (2003).

[17] M. Lindner, T. Ohlsson, and W. Winter, Nucl. Phys. **B607**, 326 (2001).

[18] Y. Chikashige, R.N. Mohapatra, and R.D. Peccei, Phys. Lett. **98B**, 265 (1981); G.B. Gelmini and M. Roncadelli, *ibid.* **99B**, 411 (1981).

[19] G. G. Raffelt, *Stars as Laboratories for Fundamental Physics* (University of Chicago Press, Chicago, 1996).

[20] M.T. Ressel and M.S. Turner, Comments. Astrophys. **14**, 323 (1990); S.D. Biller *et al.*, Phys. Rev. Lett. **80**, 2992 (1998); G.G. Raffelt, *ibid.* **81**, 4020 (1998).

[21] C.W. Kim and W.P. Lam, Mod. Phys. Lett. A **5**, 297 (1990).

[22] K. Hirata *et al.*, Phys. Rev. Lett. **58**, 1490 (1987).

[23] R.M. Bionta *et al.*, Phys. Rev. Lett. **58**, 1494 (1987).

[24] K. Zuber *et al.*, Phys. Rep. **305**, 295 (1998).

[25] M.T. Keil, G.G. Raffelt, and H.T. Janka, Astrophys. J. **590**, 971 (2003).

[26] CHOOZE Collaboration, M. Apollonio *et al.*, Phys. Lett. B **466**, 415 (1999).

[27] A.S. Dighe and A.Yu. Smirnov, Phys. Rev. D **62**, 033007 (2000).

[28] P. Vogel and J.F. Beacom, Phys. Rev. D **60**, 053003 (1999); A. Strumia and F. Vissani, Phys. Lett. B **564**, 42 (2003).

[29] MUNU Collaboration, Z. Daraktchieva *et al.*, Phys. Lett. B **564**, 190 (2003).

[30] V.D. Barger, W.Y. Keung, and S. Pakvasa, Phys. Rev. D **25**, 907 (1982); D.I. Britton *et al.*, *ibid.* **49**, 28 (1994); C.E. Piccioto *et al.*, *ibid.* **37**, 1131 (1988).

[31] J.F. Beacom, N.F. Bell, D. Hooper, S. Pakvasa, and T.J. Weiler, Phys. Rev. Lett. **90**, 181301 (2003).